

Single Top Quark Measurements at the Tevatron

J Joshi (for the DØ and CDF collaborations)

University of California, Riverside, CA 92521-0413, USA

E-mail: jjyoti@fnal.gov

Abstract. This paper reports the measurement of electroweak production of single top quarks in lepton plus jets final state by the DØ and CDF collaborations. At Fermilab's 1.96 TeV proton-antiproton collider, events are selected from several inverse femtobarns of data in the W +jets topology consistent with the signature of an isolated charged lepton (electron or muon), large missing transverse energy (\cancel{E}_T) from the W boson decay and two or more jets, at least one of them is required to be identified as originating from a bottom quark. Sophisticated multivariate analysis techniques are employed to separate the small single top quark signal from background. Both experiments measure the single top production cross section in s -channel, t -channel and $s + t$ -channel. The data is also used to extract limits on the CKM matrix element $|V_{tb}|$.

1. Introduction

The focus of this workshop, the top quark, is by far the heaviest and most interesting known particle of the standard model (SM). Top quarks are mostly produced in particle-antiparticle pairs via the strong interaction from a very high energy virtual gluon [1, 2]. The cross section at the Tevatron 1.96 TeV proton-antiproton collider is about 7.5 pb [3]. They can also be produced singly from a highly energetic virtual W boson via the electroweak interaction [4, 5]. There are three modes of single top quark production at a hadron collider [6]: t -channel production ($tqb = tq\bar{b} + \bar{t}qb$) [7], where a W boson and a b quark fuse to produce the top quark, and there are a spectator light quark and a bottom antiquark; s -channel production ($tb = t\bar{b} + \bar{t}b$) [8], where a W boson decays to a top quark and bottom antiquark. A third tW process, in which the top quark is produced together with a W boson, has a small cross section at the Tevatron [9] and is therefore not considered in this analysis. Figure 1 shows the lowest level Feynman diagrams for s - and t -channel production. Single top quark production is very distinct from $t\bar{t}$ pair production since it comes from an electroweak Wtb vertex instead of a strong gtt one. Within the SM, the single top signal allows a direct measurement of the Cabibbo-Kobayashi-Maskawa (CKM) matrix element $|V_{tb}|$ without assuming unitarity or three generations [10, 11]. Furthermore, since the top quark decays before hadronization, its polarization can be directly observed in the angular correlations of its decay products [12]. Single top processes are expected to be sensitive to several kinds of new physics. We present an improved measurement of the production rate of $tb+qb$ from DØ and CDF collaborations. We also present a measurement of the production

rates of the individual tb and tqb processes, without any theoretical assumptions on either the tb or tqb production rate or the ratio of their yields. Finally, we present a new direct measurement of $|V_{tb}|$ extracted from the measured $tb+tqb$ cross section. These results have been described in more details in [13, 14].

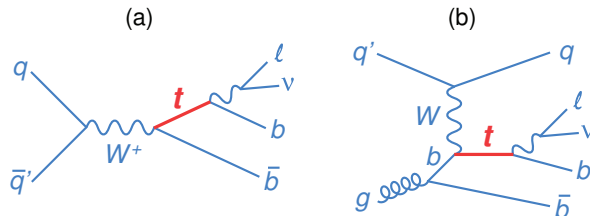


Figure 1. Lowest level Feynman diagrams for (a) tb and (b) tqb single top quark production.

2. Selecting Single Top Quark Events

The result presented in this document is based on 5.4 fb^{-1} of integrated luminosity recorded between 2002 and 2010 with the D0 detector [15], and 7.5 fb^{-1} of integrated luminosity recorded up to March 2011 with the CDF detector [16]. The data were collected with a logical OR of many trigger conditions at D0, that results in a fully efficient trigger selection for the single top signal and at CDF from the high- p_T electron/muon data stream and high- \cancel{E}_T data stream. According to the SM, the top quark is expected to decay almost exclusively into a b -quark and a W boson, as other decays are suppressed by the small values of $|V_{ts}|$ and $|V_{td}|$ matrix elements. Thus, the final state consists of an isolated electron or muon, missing transverse energy, at least one b quark jet from the decay of the top quark and a second b quark jet in the s -channel, or a light quark jet and a spectator b quark jet in the t -channel. In both cases, gluon radiation can give rise to additional jets. The data are divided into different mutually exclusive subsamples based on the jet multiplicity (2 or 3 jets), and the number of jets identified as originating from b quarks (1 or 2 b -tags) in order to take advantage of the different signal:background ratios and dominant sources of backgrounds. D0 also included events with a fourth jet because there could have been an initial-state- or final-state-radiated quark or gluon. CDF required the electron or muon to have $p_T > 20 \text{ GeV}$ and pseudorapidity $|\eta| < 1.6$. D0 required $p_T > 15$ (20) GeV and $|\eta| < 1.1$ for electrons events with 2 (3 or 4) jets, and $p_T > 15 \text{ GeV}$ and $|\eta| < 2.0$ for muons. CDF set the threshold for $\cancel{E}_T > 25 \text{ GeV}$ and \cancel{E}_T is corrected for the presence of muons and jets. D0 required \cancel{E}_T not to be aligned with the direction of the lepton or the leading jet to limit the number of events originating from multijet production entering the candidate samples and also \cancel{E}_T is required to be in the range of (20, 200) GeV for events with 2 jets and (25, 200) GeV for events with 3 or 4 jets. Events are selected that contain one jet with transverse momentum $p_T > 25$ (20) GeV and at least a second jet with $p_T > 15$ (12–20) GeV, both within pseudorapidity $|\eta| < 3.4$ (2.8) in case of D0 (CDF).

The background processes that these cuts selected are mainly from W +jets events at low multiplicity and $t\bar{t}$ pairs at high jet multiplicity, with small contributions from Z +jets, dibosons, and multijet events where one of the jets is misidentified as an electron, or a b jet decayed to produce a muon that is misleadingly reconstructed as isolated from the jet. All the background processes (except multijets) and the signal events are simulated using Monte Carlo (MC) models. Single top signal events are modeled for a top-quark mass $m_t = 172.5 \text{ GeV}$ using the COMPHEP-based next-to-leading order (NLO) MC event generator SINGLETOP [17] (D0) and POWHEG [18] (CDF). PYTHIA [19] is used to model the hadronization of any generated partons.

The $t\bar{t}$, W +jets, and Z +jets backgrounds are simulated using the ALPGEN leading-log MC event generator [20], with PYTHIA used to model hadronization. The multijet background is modeled using data. Figure 2 shows the comparisons between data and simulation for some important distributions after applying b -tagging.

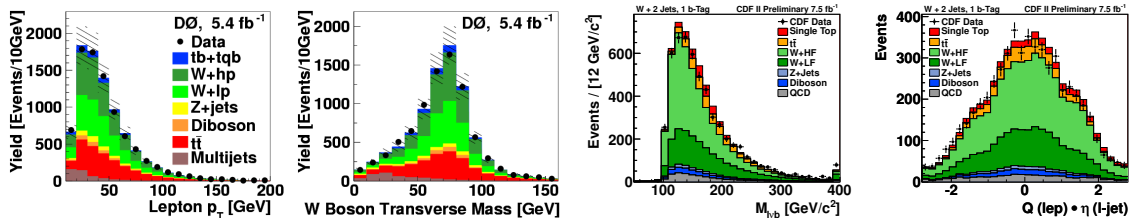


Figure 2. Comparison between the data and background model: lepton p_T and W boson transverse mass distributions from D0 analysis (first and second from left); reconstructed top quark mass and light quark jet pseudorapidity multiplied by lepton charge from CDF analysis (third and fourth from left).

3. Cross Section Measurement

The measurement of single top quark cross section present substantial experimental challenges comparing with $t\bar{t}$ production as it suffers from lower SM production rate and a large kinematically similar background. Simple counting experiments will not yield a precise measurement of the single top production cross section. Since the expected single top contribution is smaller than the uncertainty on the background, different multivariate analysis (MVA) methods are used to extract the signal. Following subsections describes the cross section measurement by D0 and CDF analyses.

3.1. $D\bar{O}$ measurement

Three different MVA techniques are applied in this analysis: (i) boosted decision trees (BDT) [21], (ii) bayesian neural networks (BNN) [22], and (iii) neuroevolution of augmented topologies (NEAT) [23]. All three methods use the same data and model for background and consider the same sources of systematic uncertainties. Each MVA method is trained separately for the two single top quark production channels: for the tb (tqb) discriminants, with tb (tqb) considered signal and tqb (tb) treated as a part of the background. Using ensembles of datasets containing contributions from SM signal and background, correlation among the outputs of the individual MVA methods is $\approx 70\%$. An increase in sensitivity can therefore be obtained by combining these methods to form a new combined discriminant that takes as inputs the three discriminant output of BDT, BNN and NEAT. Figure 3 shows the combined outputs of the tb , tqb and $tb+tqb$ discriminants, where good agreement is observed over the entire range. In these plots, the bins are sorted and merged (“ranked”) as a function of the expected signal-to-background ratio (S:B) such that S:B increases monotonically within the range of the discriminant.

The single top quark production cross section is measured using a Bayesian inference approach [24, 25]. Figure 4 shows the resulting expected and observed posterior density distributions for tb , tqb and $tb+tqb$ for the combined discriminants. All of the results are consistent with SM predictions for a top quark mass of 172.5 GeV.

3.2. CDF measurement

CDF uses artificial neural networks NeuroBayes[®] package to separate signal from background events [14]. The output distributions of s - and t -channel events are combined into one

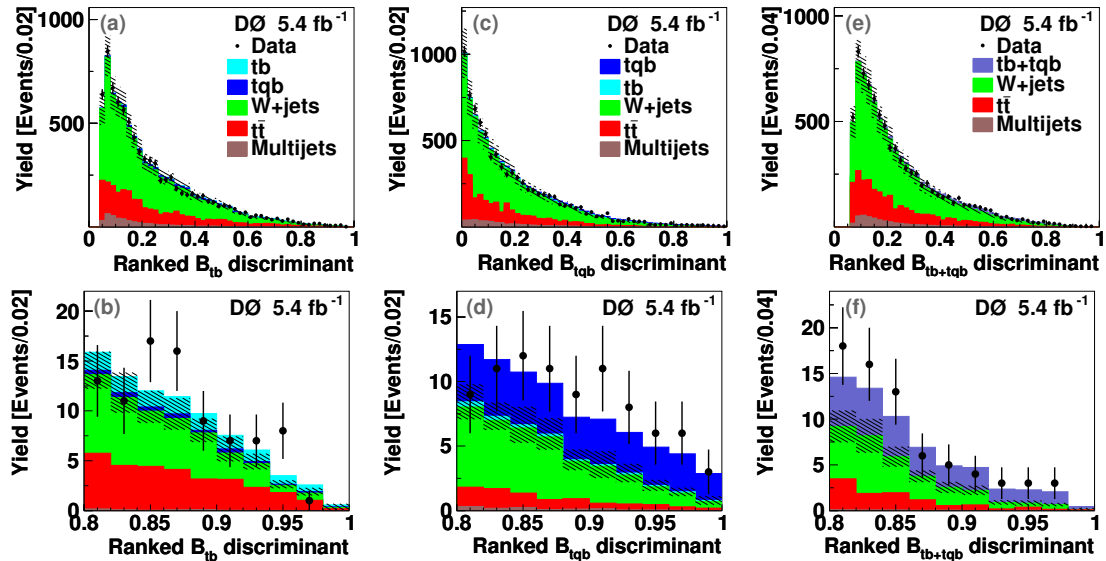


Figure 3. Distributions of the (a-b) B_{tb} , (c-d) B_{tqb} and (e-f) B_{tb+tqb} discriminant for the entire range ([0-1]) of the output, and for the signal region ([0.8-1]). The bins have been “ranked” by their expected signal-to-background ratio. The hatched bands show the 1σ uncertainty on the background prediction.

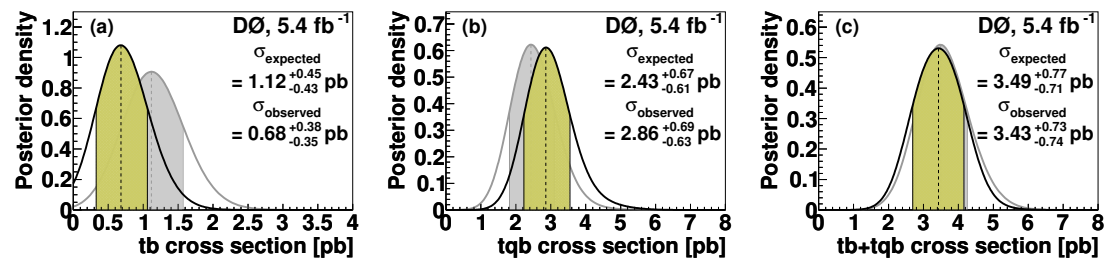


Figure 4. The expected (grey) and observed (black) posterior probability densities for (a) tb , (b) tqb , and (c) $tb+tqb$ production. The shaded bands indicate the 68% C.L.s from the peak values.

signal distribution, where the ratio between them is as predicted by the SM. The background processes whose output distributions look very similar and are hence difficult to distinguish. On this account, some of the processes are merged into one template with a ratio given by background estimation and this results in total six background templates: $t\bar{t}$, $W + HeavyFlavor$, $W + LightFlavor$, Dibosons, $Z + jets$, and multijets. NN is trained separately for s -channel (tb) and t -channel (tqb): (i) tb discriminant is trained on 2jet $2b$ -tag subsample with tqb as a part of background, and (ii) tqb discriminant is trained over rest of the subsample with tb treating as a part of background. Figure 5 (left) shows the NN discriminant distribution in the 2 and 3 jet signal region.

Using a Bayesian statistical approach, the total cross section of single top quark production assuming the SM ratio among s -channel and t -channel production is measured. The resulting posterior distribution for $s + t$ -channel is shown in Figure 5 (right).

3.3. Independent measurement of s - and t -channel cross section

To measure the individual tb and tqb production cross sections without any assumption on their values or their ratio, a two-dimensional (2D) posterior probability density is constructed as a

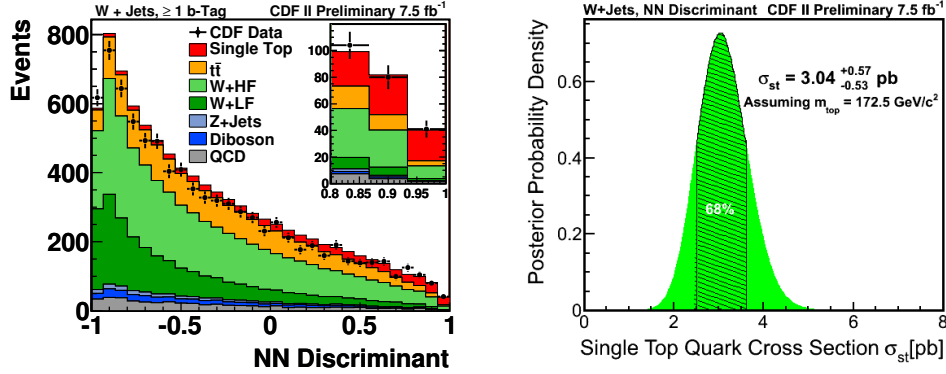


Figure 5. The resulting NN discriminant distribution (left) and the posterior probability density (right) for $tb+tbq$ production.

function of the tqb and tb production rates assuming a flat prior for each signal [26]. The resulting 2D density is shown in Figure 6, together with the points for the measured cross sections and the value expected in the SM value. From these 2D posteriors, we form a t -channel (s -channel) 1D posterior probability density function by integrating over the tb (tqb) axis, and thereby avoiding any dependency on the tb (tqb) cross section. The best-fit cross section is the one for which the posterior is maximized, and corresponds to $\sigma_s = 1.05^{+0.48}_{-0.45}$ pb (D0) and $1.81^{+0.63}_{-0.58}$ pb (CDF) and $\sigma_t = 2.32^{+0.68}_{-0.63}$ pb (D0) and $1.49^{+0.47}_{-0.42}$ pb (CDF), which are in good agreement with SM predictions [9] for the assumed $m_t = 172.5$ GeV.

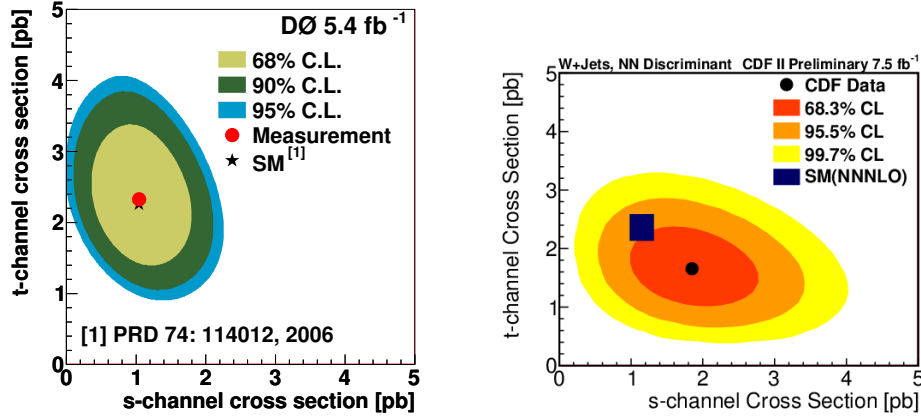


Figure 6. The posterior probability density for tqb vs. tb cross sections for D0 (left) and for CDF (right). The points corresponding to measured cross section and the SM expectation are shown.

4. $|V_{tb}|$ Measurement

The single top quark production cross section is directly proportional to the square of the CKM matrix element, $|V_{tb}|^2$, enabling us to measure $|V_{tb}|$ directly without any assumption on the number of quark families or the unitarity of the CKM matrix. Assuming the top quark decays

exclusively to Wb and that the Wtb interaction is CP -conserving, we measured the strength of $V - A$ coupling, which can be > 1 . Using the measured $tb + tqb$ cross section and restricting the prior to the SM region $[0,1]$, we extract the limit of $|V_{tb}| > 0.79$ (D0) and $|V_{tb}| > 0.78$ (CDF) at the 95% C.L. The result is also shown in Figure 7.

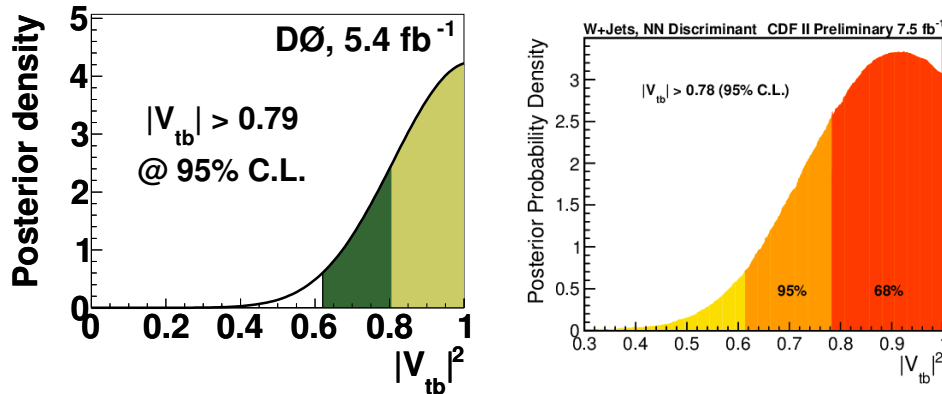


Figure 7. The posterior probability for $|V_{tb}|^2$, D0 (left) and CDF (right).

5. Summary

In summary, we have measured the single top quark production cross section using 5.4 fb^{-1} of data collected by the D0 experiment and 7.5 fb^{-1} of data collected by the CDF experiment at the Fermilab Tevatron Collider. We have also measured the individual production rates of tb and tqb processes and provided the new direct limit on the CKM matrix element $|V_{tb}|$ at the 95% C.L.

References

- [1] F. Abe *et al.* (CDF Collaboration), Phys. Rev. Lett. **74**, 2626 (1995).
- [2] S. Abachi *et al.* (D0 Collaboration), Phys. Rev. Lett. **74**, 2632 (1995).
- [3] S. Moch and P. Uwer, Phys. Rev. D **78**, 034003 (2008).
- [4] V. M. Abazov *et al.* (D0 Collaboration), Phys. Rev. Lett. **103**, 092001 (2009).
- [5] T. Aaltonen *et al.* (CDF Collaboration), Phys. Rev. Lett. **103**, 092002 (2009).
- [6] A. P. Heinson *et al.*, Phys. Rev. D **56**, 155 (1997).
- [7] S. S. D. Willenbrock and D. A. Dicus, Phys. Rev. D **34**, 155 (1986); C.-P. Yuan, Phys. Rev. D **41**, 42 (1990).
- [8] S. Cortese and R. Petronzio, Phys. Lett. B **253**, 494 (1991).
- [9] N. Kidonakis, Phys. Rev. D **74**, 114012 (2006).
- [10] N. Cabibbo, Phys. Rev. Lett. **10**, 531 (1963); M. Kobayashi and T. Maskawa, Prog. Theor. Phys. **49**, 652 (1973).
- [11] G. V. Jikia and S. R. Slabospitsky, Phys. Lett. B **295**, 136 (1992).
- [12] G. Mahlon and S. J. Parke, Phys. Rev. D **55**, 7249 (1997); G. Mahlon and S. J. Parke, Phys. Lett. B **476**, 323 (2000).
- [13] V. M. Abazov *et al.* (D0 Collaboration), Phys. Rev. D **84**, 112001 (2011).
- [14] http://www-cdf.fnal.gov/physics/new/top/confNotes/cdf10793_SingleTop_7.5_public.pdf
- [15] V. M. Abazov *et al.* (D0 Collaboration), Nucl. Instrum. Methods Phys. Res., Sect. A **565**, 463 (2006).
- [16] D. Acosta *et al.* (CDF Collaboration), Phys. Rev. D **71**, 032001 (2005).
- [17] E. E. Boos *et al.*, Phys. Atom. Nucl. **69**, 1317 (2006). We used SINGLETOP version 4.2p1.
- [18] S. Alioli *et al.*, J. High Energy Phys. **0909**, 111 (2009).
- [19] T. Sjöstrand, S. Mrenna, and P. Skands, J. High Energy Phys. **05**, 026 (2006).
- [20] M. L. Mangano *et al.*, J. High Energy Phys. **07**, 001 (2003).
- [21] L. Breiman *et al.*, *Classification and Regression Trees* (Wadsworth, Stamford, 1984).
- [22] R.M. Neal, *Bayesian Learning for Neural Networks* (Springer-Verlag, New York, 1996).

- [23] K. O. Stanley & R. Miikkulainen, *Evolving Neural Networks through Augmenting Topologies*. *Evolutionary Computation* 10(2): 99-127
- [24] V. M. Abazov *et al.* (DØ Collaboration), *Phys. Rev. D* **84**, 112001 (2011).
- [25] V. M. Abazov *et al.* (DØ Collaboration), *Phys. Lett. B* **705**, 313 (2011).
- [26] V.M. Abazov *et al.* (D0 Collaboration), *Phys. Lett. B* **682**, 363 (2010).